LJMU Research Online

McAlpine, S, Bower, RG, Harrison, CM, Crain, RA, Schaller, M, Schaye, J and Theuns, T

 The link between galaxy and black hole growth in the EAGLE simulation

http://researchonline.ljmu.ac.uk/id/eprint/6342/

Article

The link between galaxy and black hole growth in the EAGLE simulation

Stuart McAlpine,[1]★ Richard G. Bower,[1] Chris M. Harrison,[2] Robert A. Crain,[3]
Matthieu Schaller,[1] Joop Schaye[4] and Tom Theuns[1]

[1]*Institute for Computational Cosmology, Department of Physics, University of Durham, South Road, Durham DH1 3LE, UK*
[2]*Centre for Extragalactic Astronomy, Department of Physics, Durham University, South Road, Durham DH1 3LE, UK*
[3]*Astrophysics Research Institute, Liverpool John Moores University, 146 Brownlow Hill, Liverpool L3 5RF, UK*
[4]*Leiden Observatory, Leiden University, PO Box 9513, NL-2300 RA Leiden, the Netherlands*

ABSTRACT

We investigate the connection between the star formation rate (SFR) of galaxies and their central black hole accretion rate (BHAR) using the EAGLE cosmological hydrodynamical simulation. We find, in striking concurrence with recent observational studies, that the ⟨SFR⟩–BHAR relation for an active galactic nucleus (AGN)-selected sample produces a relatively flat trend, whilst the ⟨BHAR⟩–SFR relation for an SFR-selected sample yields an approximately linear trend. These trends remain consistent with their instantaneous equivalents even when both SFR and BHAR are time averaged over a period of 100 Myr. There is no universal relationship between the two growth rates. Instead, SFR and BHAR evolve through distinct paths that depend strongly on the mass of the host dark matter halo. The galaxies hosted by haloes of mass $M_{200} \lesssim 10^{11.5}$ M$_\odot$ grow steadily, yet black holes (BHs) in these systems hardly grow, yielding a lack of correlation between SFR and BHAR. As haloes grow through the mass range $10^{11.5} \lesssim M_{200} \lesssim 10^{12.5}$ M$_\odot$ BHs undergo a rapid phase of non-linear growth. These systems yield a highly non-linear correlation between the SFR and BHAR, which are non-causally connected via the mass of the host halo. In massive haloes ($M_{200} \gtrsim 10^{12.5}$ M$_\odot$), both SFR and BHAR decline on average with a roughly constant scaling of SFR/BHAR $\sim$ 10^3. Given the complexity of the full SFR–BHAR plane built from multiple behaviours, and from the large dynamic range of BHARs, we find the primary driver of the different observed trends in the ⟨SFR⟩–BHAR and ⟨BHAR⟩–SFR relationships are due to sampling considerably different regions of this plane.

Key words: galaxies: active – galaxies: evolution.

1 INTRODUCTION

Substantial effort has been dedicated both observationally and theoretically to identifying the link between the growth of galaxies and their central supermassive black holes (BHs). However, the nature of this relationship remains poorly understood. Indirect evidence of a causal connection has been suggested empirically based on the *integrated* properties of galaxies and their BH counterparts. For example, galaxy bulge mass ($M_{*,\,\mathrm{bulge}}$) and the mass of the central BH (M_{BH}) exhibit a tight, approximately linear correlation for bulge masses in excess of $M_{*,\,\mathrm{bulge}} \sim 10^{10}$ M$_\odot$ (e.g. Magorrian et al. 1998; Kormendy & Ho 2013; McConnell & Ma 2013; Scott, Graham & Schombert 2013). However, at lower bulge mass, a steeper trend has been advocated (e.g. Scott et al. 2013; Greene et al. 2016).

Additionally, the cosmic star formation rate (SFR) and black hole accretion rate (BHAR) densities broadly trace one another through time (e.g. Heckman et al. 2004; Aird et al. 2010; Madau & Dickinson 2014).

A simple interpretation for these global relationships is that the growth rates that build these properties (i.e. the SFR of the galaxy and accretion rate of the BH) are proportional throughout their evolution, thus growing the two components in concert. More complex evolutionary scenarios have also been proposed. For example, a simple time-averaged relationship built from a common fuel reservoir of cold gas (Alexander & Hickox 2012; Hickox et al. 2014), a rapid build-up of galaxy and BH mass via merger-induced starburst/quasar activity (e.g. Sanders et al. 1988; Di Matteo, Springel & Hernquist 2005; Hopkins et al. 2008) or a mutual dependence on the mass or potential of the dark matter halo (Booth & Schaye 2010, 2011; Bower et al. 2017). In these scenarios, the SFR and BHAR do not necessarily trace each other directly

★ E-mail: s.r.mcalpine@durham.ac.uk

and the observed correlations may only appear in massive galaxies due to an averaging of very different histories. Furthermore, Peng (2007) and Jahnke & Macciò (2011) go as far as to suggest there is no causal connection of any kind, with correlations only appearing as result of a random walk.

To test these scenarios, numerous observational studies have attempted to identify a direct link between the intrinsic growth rates of galaxies and their central BHs. Studies that investigate the mean SFR ($\langle$SFR$\rangle$) as a function of BHAR consistently find no evidence for a correlation for moderate-luminosity sources ($L_{2-8\,\mathrm{keV}} \lesssim 10^{44}$ erg s^{-1}; e.g. Lutz et al. 2010; Harrison et al. 2012; Mullaney et al. 2012a; Page et al. 2012; Rosario et al. 2012; Azadi et al. 2015; Stanley et al. 2015). For high-luminosity sources ($L_{2-8\,\mathrm{keV}} > 10^{44}$ erg s), however, there has been significant disagreement as to if this relation becomes positively correlated (e.g. Lutz et al. 2010), negatively correlated (e.g. Page et al. 2012) or continues to remain uncorrelated (e.g. Harrison et al. 2012; Rosario et al. 2012; Azadi et al. 2015; Stanley et al. 2015). These disparities between various works at the high-luminosity end are likely due to small number statistics and sample variance (Harrison et al. 2012), and indeed, recent studies using large sample sizes confirm the extension of a flat trend to higher luminosities (Azadi et al. 2015; Stanley et al. 2015).

A flat trend for the $\langle$SFR$\rangle$–BHAR relation could potentially be interpreted as revealing an absence of a connection between SFR and BHAR. However, studies that have investigated the mean BHAR ($\langle$BHAR$\rangle$) as a function of SFR consistently find a *positive* relationship (e.g. Rafferty et al. 2011; Symeonidis et al. 2011; Mullaney et al. 2012b; Chen et al. 2013; Delvecchio et al. 2015). Within the paradigm of a linear M_{BH}–$M_{\mathrm{bulge},\,*}$ relation due to a universal co-evolution of BH and galaxy growth, both approaches are expected to produce a consistent, similarly linear result (see Appendix A for a derivation of why this is). Hickox et al. (2014) propose a potential solution, suggesting that SFR and BHAR are connected *on average* over a period of 100 Myr, with a linear scaling. This relationship disappears when measured instantaneously owing to the rapid variability time-scale of active galactic nucleus (AGN), with respect to that of galactic star formation.

From a theoretical perspective, many simulations have focused on the growth of BHs in galaxy mergers (e.g. Di Matteo et al. 2005; Hopkins et al. 2005). Whilst both star formation and BH accretion are typically enhanced during the merger proper, the extent of the connection between SFR and BHAR pre- and post-merger event remains unclear. Neistein & Netzer (2014) demonstrate through the use of a semi-analytical model that the observed correlations between galaxies and their central BHs can be reproduced when BH growth occurs only during merger-induced starbursts. This could explain the lack of a correlation between growth rates in low-luminosity systems whilst allowing for mutual enhancement during the merger events themselves. Thacker et al. (2014) investigate the impact of various feedback models on the SFR–BHAR parameter space in a set of equal mass merger simulations. They find a complex evolution for individual systems, even when averaged over 20 Myr. Any correlation found is strongly dependant on the feedback model chosen, with the post-merger phase showing the strongest evidence for a positive connection. Using a high-resolution hydrodynamical merger suite, Volonteri et al. (2015a) find BHAR and galaxy-wide SFR to be typically temporally uncorrelated. They suggest in Volonteri et al. (2015b) that the observed discrepancy between the $\langle$SFR$\rangle$–BHAR and $\langle$BHAR$\rangle$–SFR relations seen observationally is a result of sampling two different projections of the full bivariate SFR–BHAR distribution whose build-up is constructed from different behaviours between SFR and BHAR before, during and after the merger event.

It is now possible to extend these investigations to within a full cosmological context. Using the semi-analytical code GALFORM, Gutcke et al. (2015) find a negative SFR–AGN luminosity correlation at low AGN luminosities, this then transitions to a strong positive correlation at high AGN luminosities. In the cosmological hydrodynamical simulation ILLUSTRIS, Sijacki et al. (2015) find a single trend in the SFR–BHAR relationship embedded in a large scatter, particularly in BHAR. Cosmological hydrodynamical simulations have the advantage of probing the entire galaxy population within a self-consistent variety of environments with a diverse range of accretion and merger histories. Here, we investigate to what extent galaxy and BH growth rates are connected within the 'Evolution and Assembly of GaLaxies and their Environment' (EA-GLE; Crain et al. 2015; Schaye et al. 2015)[1] simulation.[2] Adopting physical prescriptions for radiative cooling, star formation, stellar mass loss, BH accretion, BH mergers and both stellar and AGN feedback, EAGLE reproduces many observed properties of galaxies, BHs and the intergalactic medium with unprecedented fidelity (e.g. Furlong et al. 2015, 2017; Lagos et al. 2015; Rahmati et al. 2015; Schaller et al. 2015b; Schaye et al. 2015; Trayford et al. 2015, 2016; Bahé et al. 2016; Crain et al. 2017; Rosas-Guevara et al. 2016; Segers et al. 2016).

The paper is organized as follows. In Section 2, we provide a brief overview of the EAGLE simulation suite, including the subgrid model prescription and simulation output. The results are presented in Section 3. We examine the EAGLE predictions of the $\langle$SFR$\rangle$–BHAR relationship for an AGN-selected sample and the $\langle$BHAR$\rangle$–SFR relationship for an SFR-selected sample in Section 3.1, finding good agreement to recent observational findings. To investigate why these trends might be different, we explore the effect of time-averaging each growth rate and examine potential sampling biases in Section 3.2. Section 3.3 examines the influence of the host dark matter halo on both SFR and BHAR, finding that each exhibits a strong connection. Finally, in Section 4, we discuss the changing relationship between SFR and BHAR as the halo grows, and in Section 5, we present our conclusions.

2 SIMULATIONS AND SUBGRID MODEL

EAGLE is a suite of cosmological hydrodynamical simulations comprising a range of periodic volumes, numerical resolutions and physical models. The simulations are run using a substantially modified version of the *N*-body TreePM smoothed particle hydrodynamics code GADGET-3 (Springel 2005), referred to as ANARCHY (Dalla Vecchia, in preparation; see also appendix A of Schaye et al. 2015). For this study, we focus on the largest run (Ref-L0100N1504), a cubic periodic volume of 100 comoving megaparsecs (cMpc) on each side, containing 1504^3 dark matter particles of mass 9.7×10^6 M$_\odot$ and an equal number of baryonic particles with an initial mass of 1.8×10^6 M$_\odot$. The subgrid parameters are those of the EAGLE reference ('Ref-') model, described fully by Schaye et al. (2015). Cosmological parameters are those inferred by Planck Collaboration I (2014), namely $\Omega_{\mathrm{m}} = 0.307$, $\Omega_\Lambda = 0.693$, $\Omega_{\mathrm{b}} = 0.04825$, $h = 0.6777$ and $\sigma_8 = 0.8288$.

2.1 Subgrid model

Processes operating below the numerical resolution of the simulation are treated as 'subgrid', implemented as a series of physical models. A detailed description of the full subgrid prescription is given by Schaye et al. (2015), with consideration to their influence on the reference model given by Crain et al. (2015). Here, we give only a brief overview:

(i) *Radiative cooling and photoionization heating* are implemented as per Wiersma, Schaye & Smith (2009a), tracing 11 elements in the presence of the cosmic microwave background and the evolving, spatially uniform ultraviolet (UV)/X-ray background of Haardt & Madau (2001).

(ii) *Star formation* is implemented as a pressure-dependent relation that reproduces the Kennicutt–Schmidt law described by Schaye & Dalla Vecchia (2008). The subsequent *stellar mass loss* via winds of massive stars and supernovae is computed as per Wiersma et al. (2009b).

(iii) *Stellar feedback* is injected thermally and stochastically following the method of Dalla Vecchia & Schaye (2012).

(iv) *BH seeding* follows the prescription first introduced by Springel, Di Matteo & Hernquist (2005), whereby BHs are introduced as collisionless sink particles placed in the centres of dark matter haloes more massive than 1.475×10^{10} M$_\odot$, which do not already contain one. BHs enter the simulation with a seed mass $m_{seed} = 1.475 \times 10^5$ M$_\odot$ and subsequently grow via accretion of surrounding gas or mergers with other BHs.

(v) *BHs grow via accretion* of nearby material at a rate estimated from the modified Bondi–Hoyle formalism introduced in Rosas-Guevara et al. (2015). In short, the model is an extension of the spherically symmetric case of Bondi & Hoyle (1944) accounting now for the circularization velocity of the surrounding gas, capped at the Eddington limit. Contrary to Rosas-Guevara et al. (2015), we do not use an additional boost factor (α).

(vi) *AGN feedback* is implemented as a single mode, where it is injected thermally and stochastically into the surrounding interstellar medium (ISM) as per Booth & Schaye (2009). Feedback is performed assuming a single efficiency, independent of halo mass and accretion rate.

As described by Crain et al. (2015), the subgrid model parameters are calibrated to reproduce the observed galaxy stellar mass function, galaxy sizes and normalization of the $M_{BH}-M_{*, bulge}$ relation at $z \approx 0.1$.

2.2 Simulation output

2.2.1 Halo and galaxy identification

Outputs are stored as 29 'snapshots' between redshifts $z = 20$ and 0 at which the complete state of every particle is recorded. In addition, 400 data-lite 'snipshots' are produced, with a typical temporal separation of $\approx$40–60 Myr. Bound structures are identified in post-processing. First, dark matter haloes are identified using the 'friends-of-friends' (FOF) algorithm with linking length of $b = 0.2$ times the mean interparticle separation (Davis et al. 1985). Then, bound substructures (or 'subhaloes') within these haloes are identified with the SUBFIND program (Springel et al. 2001; Dolag et al. 2009) applied to the full-particle distribution (dark matter, gas, stars and BHs). We associate the baryonic component of each subhalo with a galaxy, defined to be the *central* galaxy if it hosts the particle with the minimum gravitational potential and the remainder being classified as *satellites*.

Halo mass, M_{200}, is defined as the total mass enclosed within r_{200}, the radius at which the mean enclosed density is 200 times the critical density of the Universe. Galaxy mass, M_*, is defined at the total stellar content belonging to a subhalo within a 30 pkpc spherical aperture as per Schaye et al. (2015).

2.2.2 Constructing histories of individual galaxies

In order to accurately trace the evolution of individual galaxies and their central BH for the analysis in Section 3.3, we require histories of a higher temporal resolution than is provided by the snipshot output. To do this, we follow galaxies and their central BH through cosmic time. As a galaxy descendant may have multiple progenitors, we trace the progenitor galaxy that is hosted along the 'main progenitor branch' of the merger tree as defined by Qu et al. (2017), the branch containing the greatest total mass along its history.

BHARs are recorded at each time step with a typical spacing of $\sim 10^3$–10^4 yr, yielding an 'instantaneous' rate. These can then be time-averaged over longer durations. Quoted 'instantaneous' SFRs are taken from the snapshot output, where they are computed based on the current star forming state of the gas contained within the galaxy. Time-averaged SFR histories are constructed from the stellar particles born within the main progenitor that reside in the galaxy at the present day. As these particles store both their birth time and initial mass, collectively they create a robust history of star formation for that galaxy. However, as these histories are sensitive in their resolution to the number of particles sampled, only galaxies containing more than 200 particles ($M_{*[z=0]} \approx 10^{8.5}$ M$_\odot$) are considered for this study.

Fig. 1 shows an example history of an individual galaxy's SFR (top panel) and accretion rate of the central BH (bottom panel) through cosmic time taken from the methods described above. We show each growth rate time-averaged over 5 Myr (blue and green lines) and 100 Myr (red and black lines) to highlight the large difference in variability scatter between the two time-scales. This is particularly severe for BHAR, where values recorded over short time-scales do not return a good approximation of the long-term average rate, differing in value by as much as 4 dex. We have adopted 100 Myr as our long averaging duration, as it reflects an estimate of the effective time-scale for empirical indicators of star formation using the far-infrared (FIR, the tracer of star formation for the observational studies compared to in Section 3.1, see the discussions by Neistein & Netzer 2014; Volonteri et al. 2015a). Although there are similar features between SFR and BHAR through time for this individual case (e.g. a common peak at a lookback time of 12 Gyr), globally the two histories are quite different.

2.3 The $M_{BH}-M_{200}$ relation

Fig. 2 shows the $M_{BH}-M_{200}$ relation for central galaxies at $z = 0$. We have plotted M_{BH} as a function of halo mass rather than bulge or total stellar mass due to the crucial connection that M_{200} has with both SFR and BHAR (see Section 3.3 onwards). We note that the $M_{BH}-M_*$ relation also follows the same behaviour (see fig. 1 of Barber et al. 2016) and throughout this description M_{200} and M_* can be interchanged. The overlaid two-dimensional bins are for the continued investigation in Section 3.3, where they are fully described.
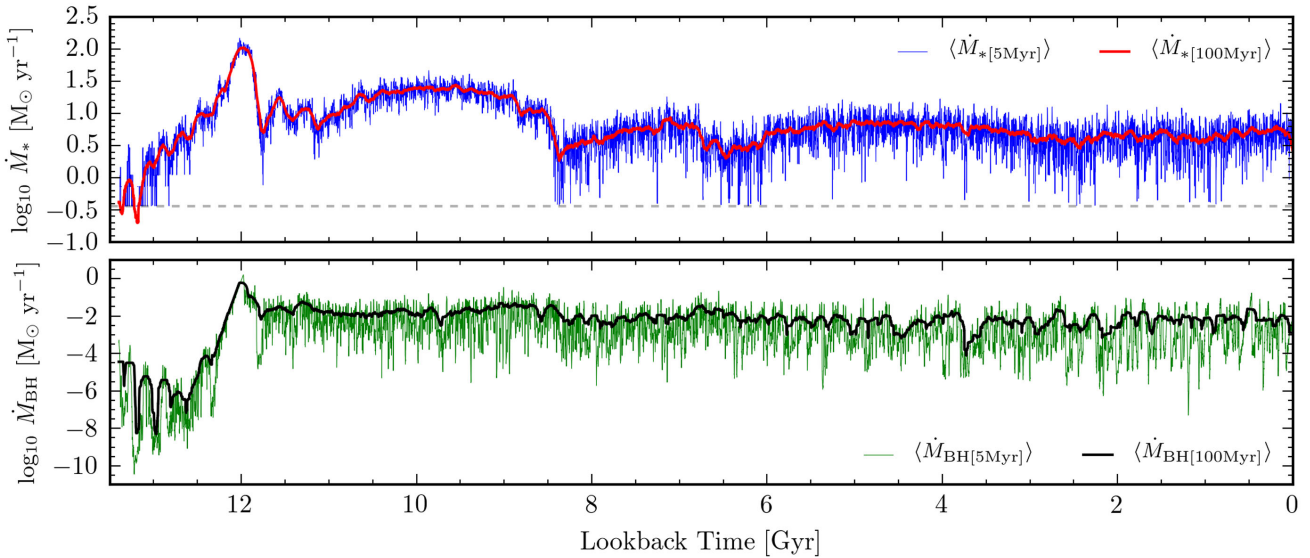
Figure 1. Galaxy (top panel) and BH (bottom panel) growth rates as a function of lookback time for an individual galaxy (GalaxyID = 20324216, $M_{200[z=0]} = 10^{13.2}$ $M_\odot$, $M_{*[z=0]} = 10^{11.1}$ $M_\odot$, $M_{BH[z=0]} = 10^{8.7}$ $M_\odot$). Blue (green) and red (black) lines show the SFR (BHAR) history averaged over 5 and 100 Myr, respectively. When averaged over short time-scales, BHARs can vary by as much as $\approx$4 dex. However, SFRs vary considerably less over the same time window ($\approx$1 dex) and generally represent values in much closer agreement to their long-term average rate. In this individual case, the long-term average trends of SFR and BHAR yield quite different evolutionary behaviours. As both the particle mass and averaging time window is finite, the minimum possible SFR sampled for a 5 Myr time-scale is shown as a dashed grey line.
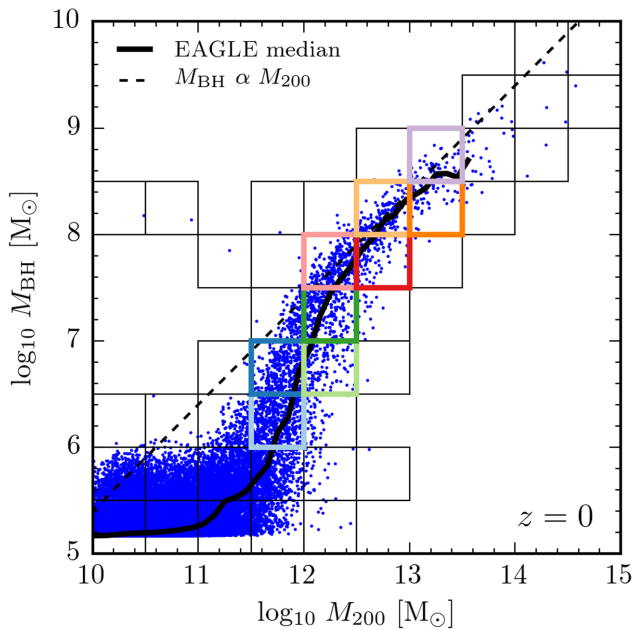

Figure 2. M_{BH}–M_{200} relation for central galaxies at $z = 0$, where M_{200} is the halo mass. Each galaxy is represented by individual blue points and the median trend is shown as a solid black line. The black dashed line shows a linear relationship, $M_{BH} \propto M_{200}$, for reference. Overlaid two-dimensional bins are 0.5 dex on each side and contain at least one galaxy. Nine of these cells are used for the continued investigation in Section 4 and are outlined in colours that relate to the histories shown in Figs 9 and 10.

The empirical relationship between BH mass and that of the classical bulge is well described by a single power law at high mass (e.g. Magorrian et al. 1998; Kormendy & Ho 2013; McConnell & Ma 2013, with gradient values of $\alpha \approx 1$–1.3 satisfying equation A1). Indeed, one of the calibration parameters of the simulation is to

match the normalization of this relationship. However, whereas traditionally this trend has been linearly extrapolated to lower mass systems, EAGLE predicts a steepening of the trend. As a consequence, the relation between BH mass and the mass of the host galaxy or halo is not well described by a single power law. Interestingly, a steeper slope at intermediate masses is supported by recent observations of bulge (or pseudo-bulge) systems (e.g. Scott et al. 2013; Greene et al. 2016). When total stellar mass is considered as the independent variable, Reines & Volonteri (2015) predict Seyfert-like systems yield and alternate M_{BH}–M_* relationship to previously measured early-type systems. However, each trend is consistent with a linear relation, with Seyfert-like systems harbouring a lower normalization.

For EAGLE, BHs in massive systems ($M_{200} \gtrsim 10^{12.5}$ $M_\odot$) follow an approximately linear trend with halo mass (compare to the black dashed black line in Fig. 2), but those hosted by haloes with mass $M_{200} \lesssim 10^{12.5}$ $M_\odot$ follow a much steeper relation and those in the lowest mass systems ($M_{200} \lesssim 10^{11.5}$ $M_\odot$) plateau at the seed BH mass.

Bower et al. (2017) argue that multiple physical processes drive the relation between M_{BH} and M_{200}. In low(high)-mass systems stellar(AGN) feedback regulates the baryonic inflow to the galaxy, suppressing BH (continued stellar) growth. There is a critical transition halo mass ($M_{200} \sim 10^{12}$ $M_\odot$, hereafter M_{crit}) separating these two regulatory regimes. Within M_{crit} haloes, neither feedback processes is dominant, and as a result BHs grow at a highly non-linear rate. These phases create the flat, supralinear and ~linear regimes of BH growth seen in the integrated quantities of Fig. 2 and have important consequences for the galaxy and BH growth rates investigated throughout this study.

2.4 Absolute calibration of SFRs

When comparing to the observed cosmic SFR density, Furlong et al. (2015) found an almost constant −0.2 dex offset for redshifts
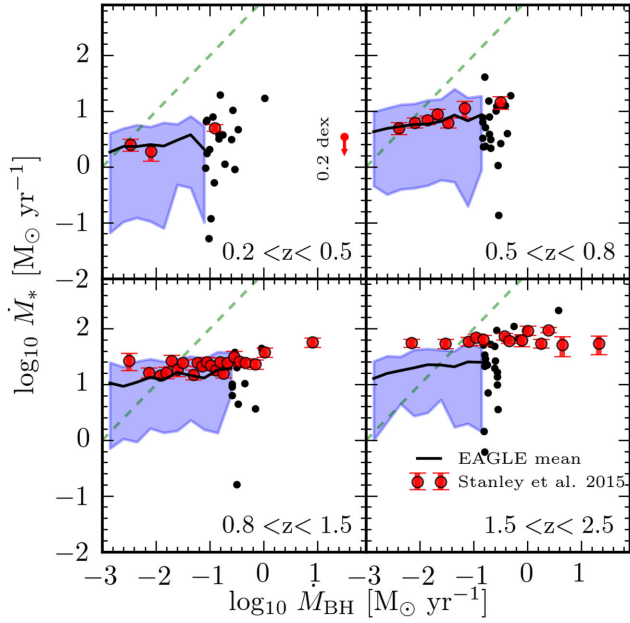
Figure 3. $\dot{M}_*$–$\dot{M}_{BH}$ (SFR–BHAR) relation for four continuous redshift ranges from $0.2 < z < 2.5$. BHARs are instantaneous and SFRs are the time-averaged rate over the 100 Myr preceding the BH event. The *mean* SFR as a function of BHAR for central galaxies is shown as a black line, with the corresponding blue shaded region, indicating the 10–90th percentile range. Bins containing fewer than 10 objects have their galaxies represented individually as black solid circles. The linear relation $\dot{M}_{BH}/\dot{M}_* = 10^{-3}$ is shown as a dashed green line and the data of Stanley et al. (2015) are represented as red circles. Fits to the EAGLE mean relations are tabulated in Table 1. The magnitude of the SFR recalibration applied to the data for all redshifts is indicated by a red arrow in the upper left-hand panel (see Section 2.4). For each redshift range, we find mean trends that are considerably flatter than a linear relation ($\gamma_{S15} \ll 1$ in equation A4).

$z \leq 3$. However, there is continued uncertainty as to the absolute calibration of SFR indicators on which these observations rely. For example, Chang et al. (2015) find upon revisiting this calibration with the addition of *Wide-Field Infrared Survey Explorer* (*WISE*) photometry to the full Sloan Digital Sky Survey (SDSS) spectroscopic galaxy sample that the SFRs of local galaxies along the main sequence are systematically lower than previously estimated by ≈0.2 dex, yielding good agreement with the EAGLE prediction (see fig. 5 of Schaller et al. 2015a).

As the observational data sets compared to in Section 3.1 utilize an earlier calibration, we *reduce* all observed SFRs by 0.2 dex. The magnitude of this recalibration is shown as a red arrow in Figs 3 and 4. This serves to remove the known global systematic offset, making it simpler to focus on the trends with BHAR that are the topic of this paper.

3 RESULTS

3.1 Comparison to observations

We begin by comparing the predicted relationship between galaxy and BH growth rates to two recent observational studies using different selection criteria. First, we explore the ⟨SFR⟩ versus BHAR relation for the *AGN-selected* sample presented by Stanley et al. (2015).
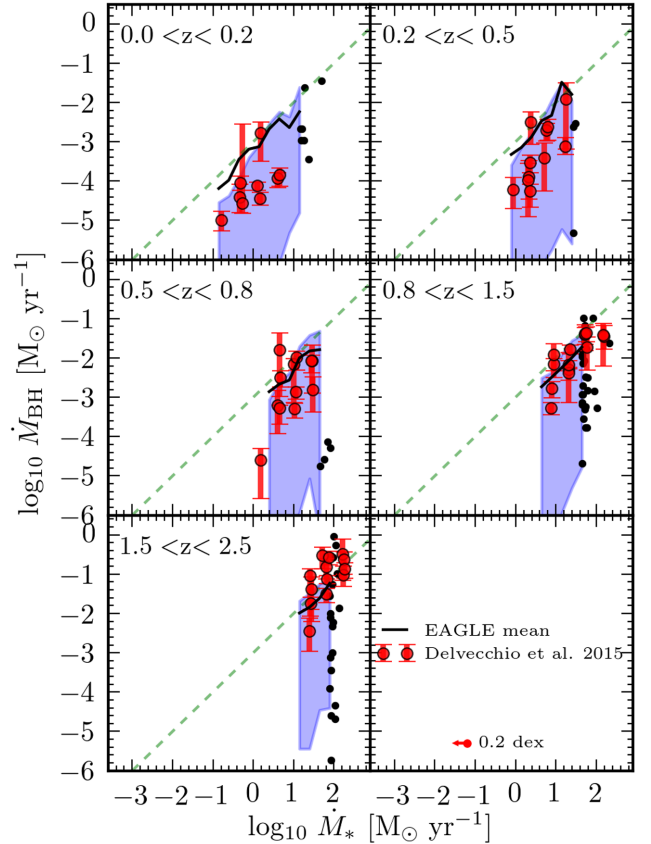

Figure 4. $\dot{M}_{BH}$–$\dot{M}_*$ (BHAR–SFR) relation for five continuous redshift ranges from $0.0 < z < 2.5$. BHARs are instantaneous and SFRs are the time-averaged rate over the 100 Myr preceding the BH event. The *mean* BHAR as a function of SFR for central galaxies is shown as a black line, with the corresponding blue shaded region indicating the 10–90th percentile range. Bins containing fewer than 10 objects have their galaxies represented individually as black solid circles. The linear relation $\dot{M}_{BH}/\dot{M}_* = 10^{-3}$ is shown as a dashed green line and the data of Delvecchio et al. (2015) are represented as red circles. Fits to the EAGLE mean relations are tabulated in Table 1. The magnitude of the SFR recalibration applied to the data for all redshifts is indicated by a red arrow in the lower right-hand panel (see Section 2.4). For each redshift range, we find gradients of the mean trend close to unity ($1/\gamma_{D15} \approx 1$) in good agreement with a linear relation.

Secondly, we explore the ⟨BHAR⟩ versus SFR relation for the *SFR-selected* sample presented by Delvecchio et al. (2015). Together they represent two of the largest sample sizes of their respective selection techniques, spanning multiple epochs. Large sample sizes such as these are key in overcoming the uncertainties inherent to low number statistics and in mitigating the potential redshift evolution biases that could be misinterpreted as an underlying trend.

As mentioned in Section 2.2.2, SFRs obtained via FIR tracers most likely probe the recent star formation history of a galaxy, rather than an instantaneous value. Therefore, the comparative SFRs of EAGLE galaxies used in the analysis of Figs 3 and 4 are the time-averaged rate over the 100 Myr, preceding the instantaneous BHAR measurement. However, when performing the equivalent analysis using the instantaneous values of SFR at the time of the BHAR measurement we find no difference in the result, attesting to the stability of star formation as a process.

Table 1. Slope (γ) and intercept (δ) of various relations satisfying equation (A4). S15 denotes the study of Stanley et al. (2015) and D15 denotes the study of Delvecchio et al. (2015). Columns 2 and 3 are the fitted values of the EAGLE mean relations investigated in Figs 3 and 4. Annotated with a * in columns 6 and 7 are the EAGLE *median* fits to the same data sets. Fits to the mean relation of the 100 Myr time-averaged growth rates from Section 3.2.1 for the same data sets are shown in columns 4 and 5. Errors on the individual mean/median EAGLE data points are taken from bootstrap resampling. Quoted fits and their associated errors were computed using the PYTHON module LMFIT.

z	γ_{S15}	$\log_{10}, \delta_{S15}$	$\gamma_{S15} \langle 100\,\mathrm{Myr}\rangle$	$\log_{10}\delta_{S15} \langle 100\,\mathrm{Myr}\rangle$	$\gamma_{S15}*$	$\log_{10}\delta_{S15}*$
$0.20 < z < 0.50$	0.13 ± 0.04	0.67 ± 0.09	0.31 ± 0.05	1.18 ± 0.14	0.14 ± 0.02	0.46 ± 0.05
$0.50 < z < 0.80$	0.15 ± 0.02	1.07 ± 0.04	0.26 ± 0.01	1.36 ± 0.04	0.12 ± 0.03	0.83 ± 0.07
$0.80 < z < 1.50$	0.12 ± 0.03	1.32 ± 0.06	0.27 ± 0.02	1.63 ± 0.04	0.14 ± 0.03	1.23 ± 0.07
$1.50 < z < 2.50$	0.16 ± 0.02	1.60 ± 0.05	0.24 ± 0.02	1.72 ± 0.05	0.16 ± 0.02	1.51 ± 0.05

z	$1/\gamma_{D15}$	$-\frac{\log_{10}\delta_{D15}}{\gamma_{D15}}$	$1/\gamma_{D15} \langle 100\,\mathrm{Myr}\rangle$	$\log_{10}\delta_{D15} \langle 100\,\mathrm{Myr}\rangle$	$1/\gamma_{D15}*$	$-\frac{\log_{10}\delta_{D15}}{\gamma_{D15}}*$
$0.01 < z < 0.25$	1.07 ± 0.10	-3.21 ± 0.05	1.06 ± 0.06	-3.29 ± 0.04	2.68 ± 0.14	-5.52 ± 0.07
$0.25 < z < 0.50$	1.13 ± 0.11	-3.30 ± 0.05	0.94 ± 0.04	-3.07 ± 0.02	2.28 ± 0.20	-5.61 ± 0.10
$0.50 < z < 0.80$	1.06 ± 0.19	-3.35 ± 0.17	1.10 ± 0.03	-3.23 ± 0.02	2.21 ± 0.33	-5.99 ± 0.29
$0.80 < z < 1.50$	1.00 ± 0.01	-3.39 ± 0.15	1.27 ± 0.03	-3.44 ± 0.03	2.48 ± 0.21	-6.53 ± 0.23
$1.50 < z < 2.50$	0.96 ± 0.16	-3.17 ± 0.24	1.37 ± 0.04	-3.60 ± 0.05	1.61 ± 0.26	-5.18 ± 0.39

3.1.1 SFR as a function of BHAR for an AGN-selected sample

The study of Stanley et al. (2015) consists of $\approx$2000 X-ray detected AGN spanning over three orders of magnitude in luminosity ($10^{42} < L_{2-8\,\mathrm{keV}} < 10^{45.5}$ erg s^{-1}) for the redshift range $z = 0.2$–2.5. To compare to the data, we convert their quoted bolometric AGN luminosities (derived from X-ray luminosities) to BHARs via

$$\dot{M}_{BH} = \frac{L_{AGN}}{\epsilon_r c^2}, \qquad (1)$$

where c is the speed of light and ϵ_r is the radiative efficiency of the accretion disc, which is assumed to be 0.1 (Shakura & Sunyaev 1973). To emulate the sample selection of this study, we choose EAGLE galaxies based on a redshift-independent detection limit of $\dot{M}_{BH} = 10^{-3}$ M$_\odot$ yr^{-1}, corresponding to $L_{AGN} \approx 10^{43}$ erg s^{-1} according to equation (1) and is equivalent to $L_{2-8\,\mathrm{keV}} \approx 10^{42}$ erg s^{-1} using the conversion methods outlined in section 3.2 of Stanley et al. (2015).

The results are presented in Fig. 3, showing the *mean* SFR as a function of BHAR, represented by a solid black line. We see that for each redshift range the gradient of the relation remains shallow (note the same dynamic range is used for both axes), ranging in values $0.1 \leq \gamma_{S15} \leq 0.2$ (see Table 1) and is in striking agreement with the 'remarkably flat' relation reported by Stanley et al. (2015). This is considerably flatter than one would predict for a linear M_{BH}–$M_{\mathrm{bulge},*}$ relation from a co-evolution of growth, which we represent as a dashed green line[3] (see Appendix A). The dynamic range of SFRs is modest, with a scatter of $\approx$1–1.5 dex for all redshifts. The normalizations of $\langle$SFR$\rangle$ in the three lowest redshift ranges ($0.2 < z < 1.5$) are in good agreement with the observational estimates (within $\approx$0.1 dex). However, the values in the highest redshift range ($1.5 < z < 2.5$) are systematically underpredicted by $\approx$0.5 dex over and above the recalibration discussed in Section 2.4. We note that this highest bin is potentially subject to the largest systematic overestimate ($\approx$0.4 dex) due to the large fraction ($\approx$80 per cent) of undetected FIR sources (included as upper limits) in the observations (see Stanley et al. 2015).

3.1.2 BHAR as a function of SFR for an SFR-selected sample

The study of Delvecchio et al. (2015) consists of $\approx$8600 star-forming galaxies detected out to $z = 2.5$. The selection limits in SFR are redshift dependent, corresponding to 0.2, 1.0, 3.0, 8.0 and 25.0 M$_\odot$ yr^{-1} for the five redshift ranges covered by this study from low to high, respectively. We note that the data points from Delvecchio et al. (2015) are segregated also in stellar mass; however, for simplicity, we make no such distinction.

The comparison is shown in Fig. 4, showing the *mean* BHAR as a function of SFR as the solid black line. Again, EAGLE shows a good consistency with the observational measurements (shown in red), only overpredicting $\langle$BHAR$\rangle$ in the lowest redshift range ($0.0 < z < 0.5$). However, Delvecchio et al. (2015) mention that the limited comoving volume of this study at low redshift could potentially exclude the most luminous sources. The behaviour of the $\langle$BHAR$\rangle$–SFR relation is quite different from the $\langle$SFR$\rangle$–BHAR relation seen in Fig. 3, adhering much closer to a linear trend. We see, uniformly, gradients close to unity ($1.0 \leq 1/\gamma_{D15} \leq 1.2$, see Table 1) in good agreement with the linear M_{BH}–$M_{\mathrm{bulge},*}$ relation expected for a co-evolution of growth, shown as a dashed green line (note again the same dynamic range is used for both axes). An additional difference is the spread of values in the minimization axis ($\dot{M}_{BH}$ for this figure). The distribution of SFRs in Fig. 4 spans a relatively narrow dynamic range, whereas here, BHARs vary as much as $\approx$4 dex in the 10–90th percentile region. In fact, the dynamic range of BHARs is so large that the small fraction of galaxies whose values dominate the mean are able to pull it outside this percentile range entirely in some places, suggesting the median to be a more suitable statistic to measure this trend.

Overall the agreement between EAGLE and the observations is excellent, particularly given that no information regarding this relation was considered during the calibration procedure. The difference in behaviour found empirically via alternate selection criteria is well reproduced by the simulation. We find, consistent with the Hickox et al. (2014) model and findings by Volonteri et al. (2015b), that $\langle$SFR$\rangle$–BHAR for an AGN-selected sample exhibits a relatively flat trend ($\gamma_{S15} \approx 0.15$), whilst that of $\langle$BHAR$\rangle$ with respect to SFR for an SFR-selected sample is substantially steeper and close to unity ($1/\gamma_{D15} \approx 1.1$). However, within the paradigm of a linear M_{BH}–$M_{\mathrm{bulge},*}$ relation created through co-evolution of growth these

---

[3] Using equation (A3) with $\beta = 1000$ (McConnell & Ma 2013).

results are both predicted to be linear (i.e. $\gamma \approx 1$ for both, see Appendix A). Therefore, either the underlying relationship itself is fundamentally non-linear, or a fuller understanding of the two processes is required. In the next section, we continue to examine potential reasons as to the cause of this difference.

3.2 Understanding the BHAR–SFR relationship

In this section, we explore two potential reasons why the $\langle \text{SFR} \rangle$–BHAR and $\langle \text{BHAR} \rangle$–SFR trends are not each consistent with a linear relationship. We examine the hypothesis that (1) growth rates have an underlying linear connection only on average, which is masked when the unstable growth rate is observed instantaneously, and (2) how selection biases due to the inability to probe the complete SFR–BHAR plane may play a role.

3.2.1 A time-averaged SFR–BHAR connection

Hickox et al. (2014) suggested that an underlying correlation held between a stable (galactic star formation) and unstable (BH accretion) process *on average* could be washed out if the unstable property is measured instantaneously. That is to say, if one could observe X-ray luminosities of AGN sources over prolonged periods, the underlying relationship between the two properties would begin to emerge. Indeed, with a simple model that assumes SFR and BHAR are connected on average with a linear scaling over a period of 100 Myr, Hickox et al. (2014) reproduce the empirical behaviours of both the $\langle \text{SFR} \rangle$–BHAR and $\langle \text{BHAR} \rangle$–SFR relationships whilst retaining a scenario consistent with a linear co-evolution between galaxies and their central BHs. Whilst it is not possible to test observationally due to the length of these time-scales, we are able to test this hypothesis using the simulation.

Fig. 5 is similar to the upper left-hand panel of Fig. 3. The region in blue, with the black solid line, shows the original analysis of the $\langle \text{SFR} \rangle$–BHAR relation for the redshift range $0.2 < z < 0.5$ using instantaneous BHARs and SFRs that are time-averaged 100 Myr before the BH event. Overlaid in red, with the mean represented by a dashed line, is the same selection of galaxies (i.e. instantaneous $\dot{M}_{\text{BH}} > 10^{-3}$ M$_\odot$ yr^{-1}) with each growth rate now time-averaged over 100 Myr. Interestingly, although the high BHARs shift systematically to lower values on average,[4] both the dynamic range and slope of the mean remain broadly consistent with their instantaneous equivalents ($\gamma_{\text{S15}} \rightarrow \gamma_{\text{S15}(100\,\text{Myr})} = 0.2 \rightarrow 0.3$, see Table 1). This behaviour remains for each redshift range explored by Stanley et al. (2015) (see Table 1). An alternate approach is to select galaxies in excess of $\dot{M}_{\text{BH}} = 10^{-3}$ M$_\odot$ yr^{-1} on average (rather than instantaneously as done above) or indeed to prolong the averaging time-scale to >100 Myr. However in each case and for all redshift intervals, the gradient values remain well below unity ($0.30 < \gamma_{\text{S15}(100\,\text{Myr})} < 0.55$). This leads us to conclude that the average galaxy and BH growth rates for an AGN-selected sample do not harbour an underlying global linear relationship.

3.2.2 Sampling different regions of the entire SFR–BHAR plane

As observational surveys are subject to various flux limitations, they can only sample particular regions of the full SFR–BHAR plane. If

[4] The shift (≈ 0.5 dex) to lower values in BHAR when averaging over 100 Myr arises due to the most luminous 'detections' commonly residing in peaks of the accretion rate history.
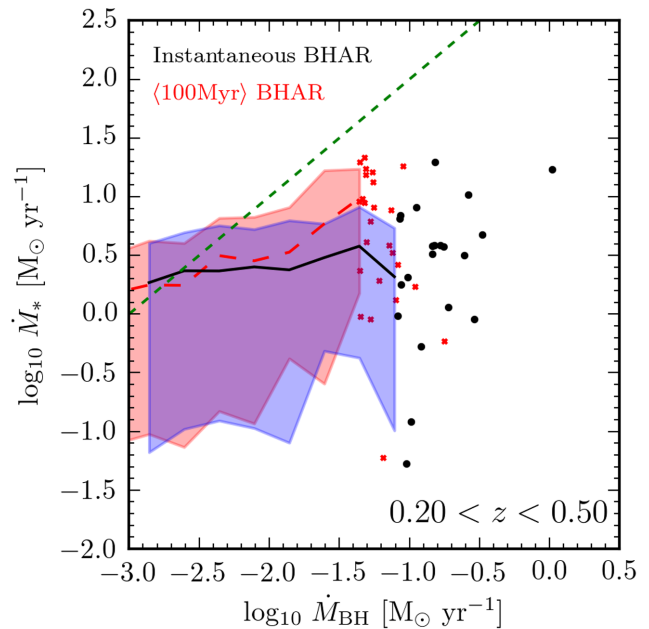

Figure 5. Blue region: a replica of the upper left-hand panel in Fig. 3 (see caption for description of contents). Here, BHARs are instantaneous and SFRs are the time-averaged rate over the 100 Myr preceding the BH event. Red region: we repeat the analysis for the same central galaxies satisfying the Stanley et al. (2015) selection criteria (instantaneously, blue region); however, now both SFR and BHAR are time-averaged over the same 100 Myr period. Fits to the time-averaged mean relations are shown in Table 1 (denoted with $\langle 100\,\text{Myr} \rangle$). We find that even when both growth rates are time-averaged over 100 Myr, an AGN-selected sample does not revert to a linear relationship between $\dot{M}_*$ and $\dot{M}_{\text{BH}}$.

the global underlying relation is linear, and each property exhibits a moderate scatter, each subsample should also return a linear result. However, as the findings of previous sections do not to support an underlying linear relation, and because the scatter is large, it is important to investigate the effect of this sampling.

Fig. 6 shows the complete SFR–BHAR plane for all central galaxies at $z = 1$. In order to eliminate any potential bias incurred via redshift evolution in either growth rate, we consider a discrete redshift rather than the continuous ranges of Section 3.1. Each data point represents the *instantaneous* state of a single galaxy and its central BH, coloured by the halo mass. Values that are below 10^{-8} M$_\odot$ yr^{-1} for $\dot{M}_{\text{BH}}$ and 10^{-3} M$_\odot$ yr^{-1} for $\dot{M}_*$ are treated as 'zero' and are clipped to these values. The approximate flux limit of the AGN-selected sample by Stanley et al. (2015) is shown as a solid vertical line and the approximate flux limit of the SFR-selected sample by Delvecchio et al. (2015) is shown as a horizontal solid line.

It is further apparent that the global relationship between SFR and BHAR is not simply linear (reference with the dashed green line). Instead, a complicated relationship arises due to an amalgamation of three distinct behaviours of BH growth dependent on the mass of the host dark matter halo (see next section). It is therefore crucial to consider the particular region sampled before arriving at a particular conclusion. AGN-selected samples, such as that of Stanley et al. (2015), currently probe a relatively limited region at the tip of the SFR–BHAR plane. With the exception of a few sources with rates $\dot{M}_* \ll 1$ M$_\odot$ yr^{-1}, galaxies satisfying this selection criteria are distributed over a relatively narrow range of SFRs. As such, each bin of BHAR yields a very similar value of $\langle \text{SFR} \rangle$, creating an approximately flat trend. SFR-selected samples, such as that of
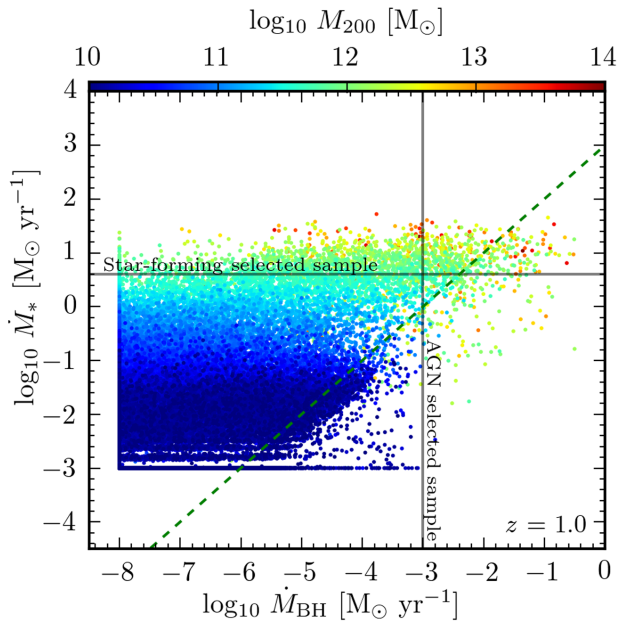
Figure 6. $\dot{M}_*$–$\dot{M}_{BH}$ (SFR–BHAR) relation for central galaxies at $z = 1$. Growth rates are *instantaneous* and coloured by the mass of the halo (M_{200}). Values that are below 10^{-8} M$_\odot$ yr^{-1} for $\dot{M}_{BH}$ and below 10^{-3} M$_\odot$ yr^{-1} for $\dot{M}_*$ are clipped to these limits. The approximate flux limits of Stanley et al. (2015) and Delvecchio et al. (2015) investigated in Section 3.1 are shown as vertical and horizontal solid lines, respectively, highlighting the different regions of the full distribution that these surveys are able to probe. The dashed green line indicates the linear relation $\dot{M}_{BH}/\dot{M}_* = 10^{-3}$.

Delvecchio et al. (2015), sample a not too dissimilar distribution of SFRs (this time due to the flux limit), however, the distribution of BHARs is much wider. This in turn yields a steeper relation. We note that whilst the mean SFR provides a good proxy of the median SFR for an AGN-selected study (compare columns 3 and 6 of Table 1), the mean BHAR for an SFR-selected study is not a good proxy of the median value due to the distribution of BHARs having such a large scatter (compare columns 8 and 10 of Table 1). Although only the results from $z = 1$ have been shown here, when investigated we find the results remain true independent of redshift.

Therefore, we conclude that the different behaviour found for the ⟨SFR⟩–BHAR and ⟨BHAR⟩–SFR relations recovered by observational studies is due to sampling considerably different regions of the full (not universally linear) SFR–BHAR plane. We now continue to investigate the nature of this relationship in the EAGLE simulation and its evolution through time.

3.3 The connection to the host dark matter halo

The relationship between SFR and BHAR seen in Fig. 6 is complicated, seemingly not adhering to a simple universal trend. However, there is evidence that each property has a link with the mass of the host dark matter halo, highlighted in the change of the data point colours, which transition smoothly from blue to red with increasing SFR, and systematically shift rightwards in BHAR (with a large scatter) at high halo mass.

To examine this in more depth, we subcategorize the $z = 1$ central galaxies into five continuous ranges of halo mass, showing the growth rates in Fig. 7. Here we find, in fact, that the global make-up of the SFR–BHAR plane in Fig. 6 is resolved into a collection of two-dimensional strips, wide in their dynamic range of BHAR
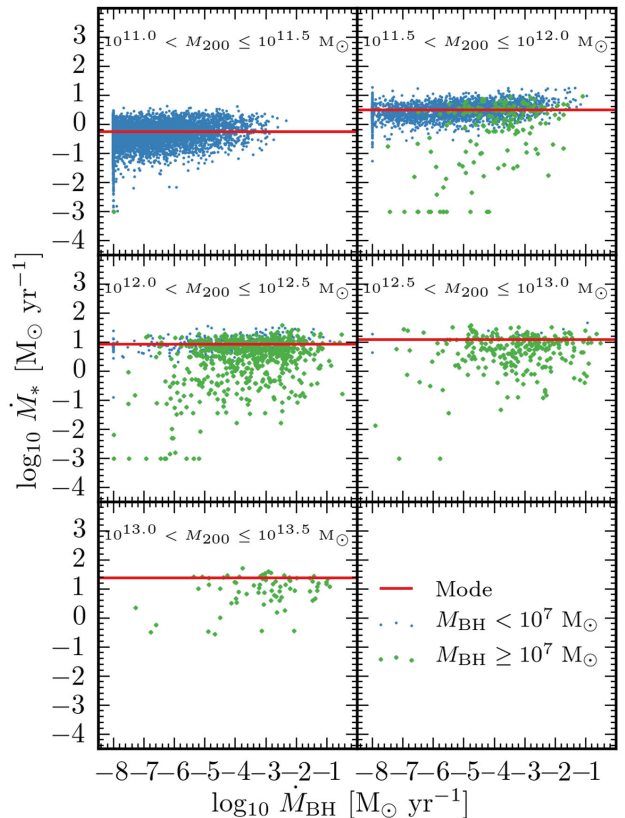

Figure 7. Growth rates at $z = 1$ (from Fig. 6) for central galaxies separated into five continuous halo mass ranges. Points are coloured green if a galaxy hosts a massive BH ($M_{BH} \geq 10^7$ M$_\odot$) and blue otherwise. The characteristic SFR for a given halo mass bin (classified as the mode of the distribution) is shown as a horizontal solid red line. Each range of halo mass yields a relatively narrow distribution of SFRs (1–2 dex) and much wider distribution of BHARs (up to 8 dex). Larger haloes are associated with larger characteristic SFRs and have a higher fraction of BHARs > 10^{-4} M$_\odot$ yr^{-1}. Galaxies harbouring SFRs far below the characteristic rate all contain massive BHs (green points) and have likely recently undergone a violent episode of AGN feedback reducing the current star-forming capability of the system.

($\approx$4–6 dex) yet generally much more compact in their SFR ($\approx$1–2 dex). Each strip hosts a characteristic value of SFR (defined as the mode of the distribution, shown as a horizontal solid red line) that continuously increases with increasing halo mass. This is in line with the 'star-forming main sequence', where galaxies of increased stellar mass are seen to host larger SFRs (e.g. Elbaz et al. 2007). Interestingly, the rate of change with M_{200} for this characteristic SFR does not remain constant, initially increasing by $\Delta\dot{M}_* \approx 1$ dex in the range $10^{11.0} < M_{200} \leq 10^{12.0}$ M$_\odot$ and reducing to almost zero in the regime $10^{12.5} < M_{200} \leq 10^{13.5}$ M$_\odot$. This is potential evidence that SFRs in massive systems are not keeping pace with the increasing baryonic inflow rates for increasing halo mass at fixed redshift (e.g. Correa et al. 2015). BHARs show a less continuous behaviour, however, broadly categorized by two rudimentary states: BHs residing in haloes below $\approx 10^{11.5}$ M$_\odot$ are typically accreting at a 'low' rate ($\dot{M}_{BH} \ll 10^{-4}$ M$_\odot$ yr^{-1}); BHs residing in haloes more massive than $\approx 10^{12.5}$ M$_\odot$ tend to be accreting at a 'high' rate ($\dot{M}_{BH} > 10^{-4}$ M$_\odot$ yr^{-1}). The fraction of galaxies with $\dot{M}_{BH} \geq 10^{-4}$ M$_\odot$ yr^{-1} for a given halo mass bin is $\approx$3 per cent, 21 per cent, 55 per cent, 70 per cent and 78 per cent from $10^{11.0} < M_{200} \leq 10^{11.5}$ M$_\odot$ to $10^{13.0} < M_{200} \leq 10^{13.5}$ M$_\odot$, respectively. Those in
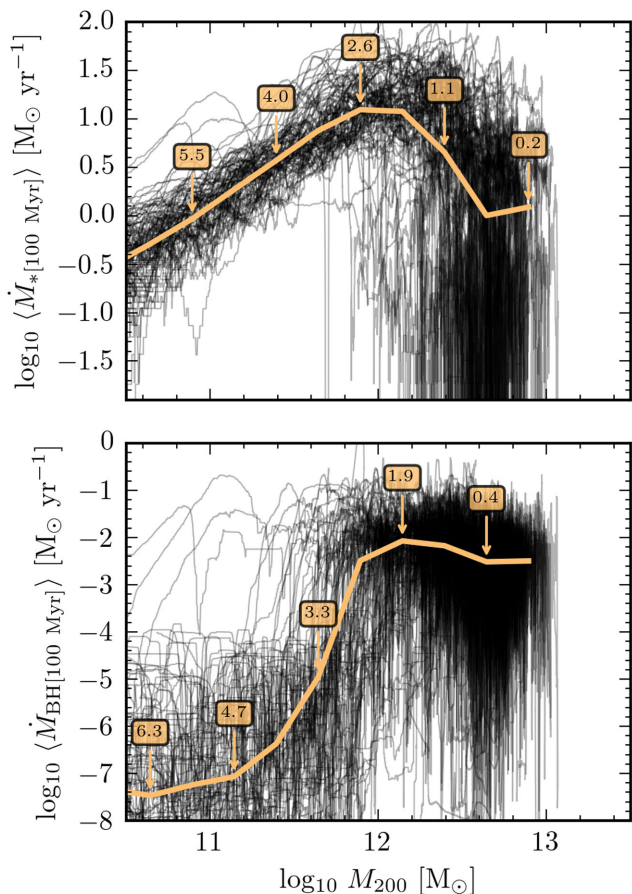
Figure 8. The evolutionary history of SFR (top panel) and BHAR (bottom panel) as a function of halo mass for all galaxies that come to reside in the $10^{12.5} < M_{200} < 10^{13.0}$ M$_\odot$, $10^{8.0} < M_{BH} < 10^{8.5}$ M$_\odot$ two-dimensional bin of Fig. 2 at $z = 0$ (outlined in yellow). Each black line is an individual history. The orange line shows the median trend, annotated with the median redshift at which these galaxies were hosted in haloes of that mass. For each panel, growth rates are time-averaged over 100 Myr as to overcome the noise induced when considering instantaneous rates. We see very different evolutionary behaviour for SFR and BHAR as the halo grows. SFRs initially rise and then decline, centred around $M_{200} \sim 10^{12}$ M$_\odot$. BHARs similarly transition from a low to high rate around this halo mass.

haloes between the mass range $10^{11.5}$–$10^{12.5}$ M$_\odot$ are in an intermediate state.

A fraction of galaxies hosted by haloes with $M_{200} \gtrsim 10^{11.5}$ M$_\odot$ harbour extremely low or even zero SFRs. As all of these galaxies host massive BHs ($M_{BH} \geq 10^7$ M$_\odot$, green dots), we are most likely seeing the effect of recent episodes of violent AGN feedback that have severely reduced the current star-forming capabilities of these systems. The cause, prevalence and impact of these feedback events will be the subject of a future paper.

We now investigate if the growth rate to halo connection evolves. To do this we return to the M_{BH}–M_{200} relation shown for $z = 0$ in Fig. 2. The population is subdivided into two-dimensional bins, 0.5 dex on a side and outlined as squares. Here, we investigate nine bins that lie along the median track through a continuous range spanning $10^{11.5} < M_{200} < 10^{13.5}$ M$_\odot$ in halo mass and $10^{6.0} < M_{BH} < 10^{9.0}$ M$_\odot$ in BH mass, each outlined with a unique colour to reference their histories in Figs 8–10.

Fig. 8 shows the evolution of the time-averaged SFR (top panel) and time-averaged BHAR (bottom panel) as a function of halo mass
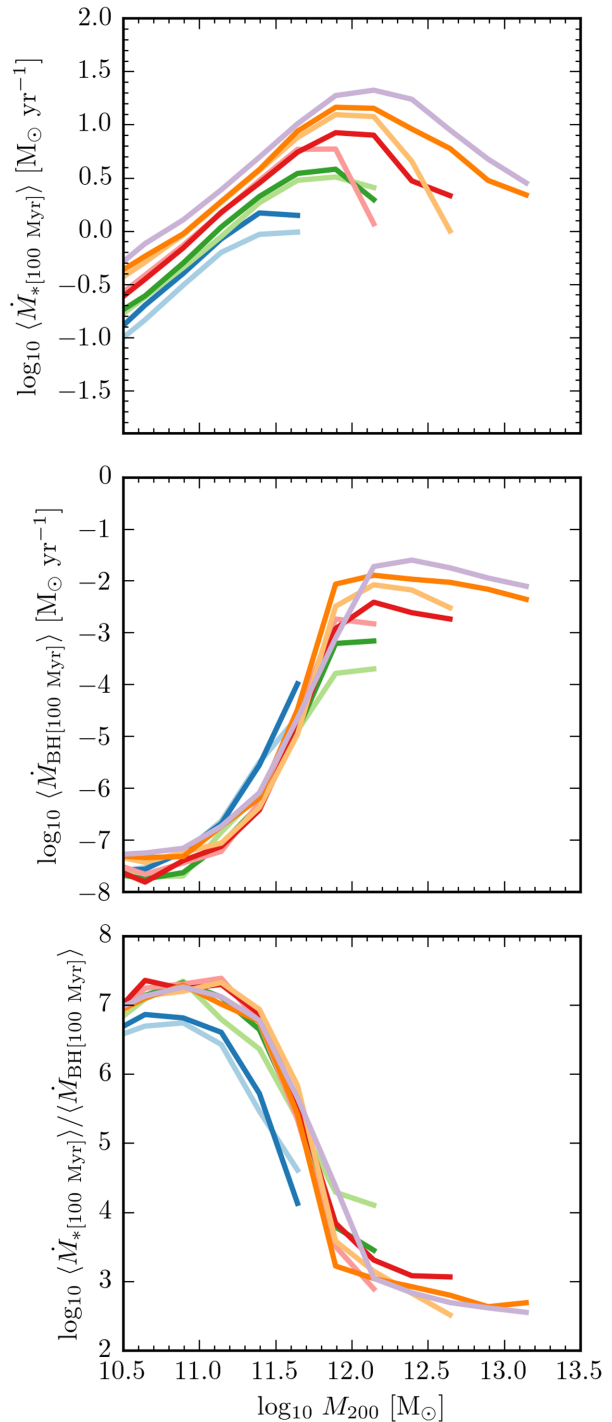

Figure 9. Top two panels: a continuation of the analysis in Fig. 8 to each of the nine chosen two-dimensional bins of Fig. 2. The lines are the median track, with the colour corresponding to the outline in Fig. 2. Regardless of where a galaxy is located on the M_{BH}–M_{200} plane at the present day, both the galaxy and its central BH evolve similarly, though different from each other. The change in normalizations between the histories is due to the declining baryonic inflow rates with decreasing redshift for a fixed halo mass. Bottom panel: the median ratio between the SFR and BHAR from the two panels above. SFRs are initially dominant by many orders of magnitude in low-mass haloes ($M_{200} \lesssim 10^{11.5}$ M$_\odot$), coming to plateau at an approximately constant value of $\sim 10^3$ in high-mass haloes ($M_{200} \gtrsim 10^{12.5}$ M$_\odot$).
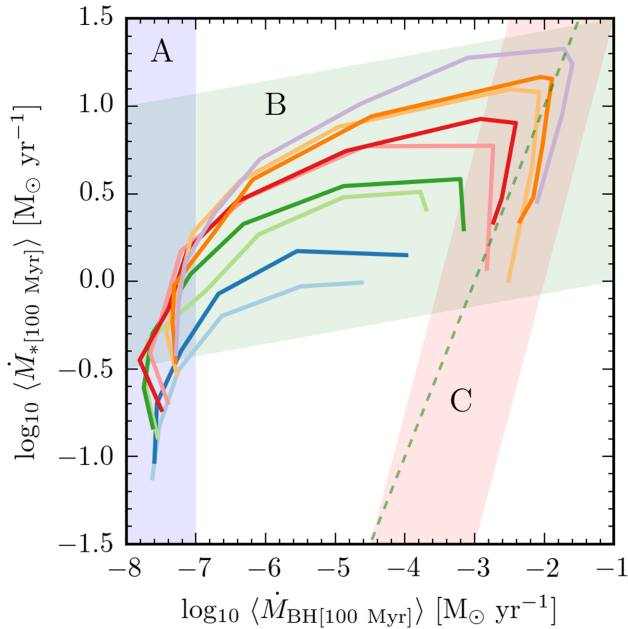
Figure 10. Each line shown here equates the median trends from the top two panels of Fig. 9 to give the 100 Myr average SFR as a function of the 100 Myr average BHAR (in equal spacings of halo mass). Region A (shaded blue) corresponds to galaxies hosted by haloes with $M_{200} \lesssim M_{crit}$. Galaxies in this regime increase their SFR with increasing halo mass, whilst BHARs remain negligible on average. As haloes reach $\sim M_{crit}$ in region B (shaded green), SFRs continue to rise; however, the BH growth increases by many orders of magnitude over this narrow halo mass range. For haloes in excess of $\gtrsim M_{crit}$ shown in region C (shaded red), we see a reduction for both SFR and BHAR on average, yielding an approximately constant scaling between the two growth rates (compare to dashed green line that shows the linear relation $\dot{M}_{BH}/\dot{M}_* = 10^{-3}$).

for all galaxies that come to reside in one of these two-dimensional bins at the present day (each solid black line is an individual history). We time-average both SFR and BHAR over 100 Myr in order to remove the inherent noise when considering instantaneous growth rates, and unveil the average trend. To eliminate galaxies that were previously classified as satellites of a more massive halo, we only consider central galaxies that have evolved monotonically in their halo mass (this excludes only ≈1 per cent of the $z = 0$ centrals population). We see that although individual histories can be quite different, on average galaxies and their central BHs do follow a well-defined path. The median SFR and BHAR of this population subset for a given halo mass are overplotted in yellow, annotated by the median redshift at which they were hosted by haloes of that particular mass. As expected, an increasing halo mass corresponds to a decreasing redshift.

There is a striking difference in behaviour seen between the two growth rates as the halo grows. Initially, the SFR increases steadily with halo mass. As the halo grows more massive than ≈10^{12} M$_\odot$ the SFRs begin to fluctuate between high and low values, yet overall there is a gradual decline of the median trend after this mass. Similarly, BHARs also change their behaviour around ≈10^{12} M$_\odot$, rapidly transitioning from a low ($\dot{M}_{BH} \ll 10^{-4}$ M$_\odot$ yr^{-1}) to high ($\dot{M}_{BH} > 10^{-4}$ M$_\odot$ yr^{-1}) rate. As with SFRs, BHARs decline a similar amount after the halo mass ≈10^{12} M$_\odot$ (note the many orders of magnitude difference in the scale of the growth rate axis between the two panels). We interpret therefore, given that the decline of SFR coincides with the peak of the rapid increase in BHAR, that

AGN feedback is impeding the continued rise of SFRs in the most massive systems (see Fig. 1 for an individual example of SFR reduction after the peak AGN activity at lookback time ≈12). We note that the decrease in halo mass accretion rate with declining redshift and the dependence of halo cooling rates on halo mass will play *additional* roles in shaping these histories. However, given the severity of the SFR reduction seen immediately after the BHAR peak, AGN feedback appears to be a dominant factor in hindering further galaxy growth.

Fig. 9 extends this analysis to each of the highlighted two-dimensional bins in Fig. 2, now showing only the median lines for clarity. Remarkably, the evolutionary behaviour is similar regardless of the final position in the M_{BH}–M_{200} plane. The normalization of each history is set by the evolving baryonic inflow rate at fixed halo mass. As this rate decreases with redshift (e.g. Correa et al. 2015), so does the normalization of both the SFR and BHAR seen here (as each population reaches a particular halo mass at different times). We include also in the bottom panel of Fig. 9 the median ratio between SFR and BHAR shown in the two panels above. This shows that galaxy growth is dominant over BH growth by many orders of magnitude in low-mass haloes ($M_{200} \lesssim 10^{11.5}$ M$_\odot$). As BHARs settle to their 'high' rate in haloes of a mass above $M_{200} \sim 10^{12}$, the ratio between SFR and BHAR plateaus to an approximately constant value of $\sim 10^3$. Note that the trends of both Figs 8 and 9 are not directly observable as they rely on median time-averaged growth rates in both SFR and BHAR of 100 Myr whilst also being binned by halo mass.

4 DISCUSSION

Throughout this investigation, we have consistently found no evidence supporting a simple underlying relationship between the rate of a galaxy's star formation and the accretion rate of its central BH. Instead, a mutual dependence of each property upon the mass of the host halo yields a more complex connection. It is interesting to examine, then, how the relation between the SFR and BHAR evolves for individual objects. In the following discussion, we will provide a physical interpretation based on the Bower et al. (2017, hereafter B17) model for BH growth (for a similar interpretation on the importance of supernova feedback to BH growth see Dubois et al. 2015; Habouzit, Volonteri & Dubois 2017). However, we stress the simulation results are themselves independent of any physical interpretation.

Fig. 10 equates the median trends of the SFR and BHAR histories shown in Fig. 9. This specifies the 100 Myr average SFR as a function of the 100 Myr average BHAR in equal spacings of halo mass. Three distinct trends between SFR and BHAR emerge as the halo evolves: the *stellar feedback regulated* phase (shaded blue), the *non-linear BH growth* phase (shaded green) and the *AGN feedback regulated* phase (shaded red).

(i) *Region A – the stellar feedback regulated phase.* From the time of their seeding until they are hosted by haloes of mass $M_{200} \sim 10^{11.5}$ M$_\odot$ the BH accretion rates are negligible ($\dot{M}_{BH} \leq 10^{-6}$ M$_\odot$ yr^{-1} on average). By contrast, SFRs increase steadily with halo mass. The combination of these two behaviors produce the uncorrelated (yet causally connected) ~vertical trend in region A, creating an imbalance of growth within these systems. As a result, BHs remain close to their seed mass, whilst the halo/galaxy continues to grow around them (see the low-mass region of Fig. 2).

B17 interpret galaxies in this regime as being in a state of regulatory equilibrium. Energy injected by stars heats the ISM within

the stellar vicinity, ejecting it and causing it to rise buoyantly in the halo. This in turn creates an outflow of material balancing the freshly sourced fuel from the cosmic web, and as such prevents large gas densities from building up within the inner regions of these low-mass galaxies. Such low densities, coupled with the relatively low-mass BHs living within these galaxies (BHAR $\propto M_{\mathrm{BH}}^2$), ensure that BHs fail to grow substantially.

(ii) *Region B – the non-linear BH growth phase*. Both galaxies and BHs grow through the halo mass range $M_{200} \sim 10^{11.5}$–$10^{12.0}$ M$_{\odot}$. However, whereas the SFRs continue to increase steadily with increasing halo mass, BHs rapidly transition to a non-linear phase of growth. This creates a highly non-linear *indirect* correlation between SFR and BHAR, connected through the host halo mass.

The physical interpretation posited by B17 is that haloes that grow to the transition mass, M_{crit}, have become sufficiently massive to stall the regulatory outflow. Because of (what is now) the haloes' hot coronae, heated gas ejected by stellar feedback loses the capability to rise buoyantly and therefore returns to the galaxy centre. Densities in the central regions of the galaxy are no longer kept low and a 'switch' to non-linear BH growth is triggered.

(iii) *Region C – the AGN feedback regulated phase*. For haloes with masses above $M_{200} \sim 10^{12}$ M$_{\odot}$ SFRs and BHARs both decline on average, correlated with an approximately linear trend (compare to green dashed line, see also the bottom panel of Fig. 9).

B17 argue that BHs in these haloes have become sufficiently massive (through their rapid non-linear growth) to efficiently regulate the gas inflow on to the galaxy themselves via AGN feedback. This again creates an equilibrium state, for which a fluctuating low level of (specific) BH accretion is maintained, keeping the outer halo hot and evaporating much of the new cold material trying to enter the system from the intergalactic medium.

Galaxies and their central BHs within the EAGLE simulation transition through multiple stages of growth as their host dark matter halo evolves, creating three distinct behaviours between SFR and BHAR. This is a stark contrast to a simple model where SFR and BHAR correlate globally via a linear relation, on average and for all halo masses. Whilst the underlying trend is only revealed when each growth rate is time-averaged (given the inherent noise of instantaneous growth rates), we only find an approximately linear correlation for the most massive systems ($M_{200} \gtrsim 10^{12.5}$ M$_{\odot}$).

In this paper, we have emphasized the role of the halo and how its interaction with both SFR and BHAR shapes the growth rate relationship. However, additional factors may also contribute to the form this relationship takes. For example, Volonteri et al. (2015b) find, using a suite of isolated merger simulations at fixed halo mass, that alternate behaviours between SFR and BHAR before, during and after the merger proper collectively contribute to form a complex two-dimensional plane. Additionally, Pontzen et al. (2017) reveal the particular importance differing merger histories can have on significantly altering the growth rate history of both that of the galaxy and the central BH. However, the global influence of mergers upon galaxy and BH growth rates in a full cosmological context remains open for debate, and will be the subject of a future paper.

5 CONCLUSIONS

We have investigated the relationship between the galaxy SFR and the BHAR of the central BH using the EAGLE cosmological hydrodynamical simulation. Our main conclusions are as follows:

(i) We compared EAGLE predictions to two recent observational studies in Figs 3 and 4. The simulation reproduces both the flat trend of the mean SFR ($\langle$SFR$\rangle$) as a function of BHAR found in the AGN-selected study of Stanley et al. (2015) and the approximately linear trend of the mean BHAR ($\langle$BHAR$\rangle$) as a function of SFR found in the SFR-selected study of Delvecchio et al. (2015).

(ii) There is a moderate difference in the $\langle$SFR$\rangle$–BHAR relationship when time-averaging each growth rate over a 100 Myr period for an AGN-selected study (Fig. 5). However, this change was not found to be sufficient as to revert the trend to an underlying linear relationship as has been proposed by previous theoretical studies.

(iii) Examining the complete $z = 1$ SFR–BHAR plane in Fig. 6, we found no evidence for a simple universal global relationship between the two instantaneous growth rates. The difference between the trends found for the $\langle$SFR$\rangle$–BHAR and $\langle$BHAR$\rangle$–SFR relations from AGN and SFR selections, respectively, is due to sampling different regions of this complex plane. The complexity of this plane results from both the rate of galactic star formation and the accretion rate of the central BH holding an evolving connection to the host dark matter halo (Fig. 7).

(iv) For a discrete redshift, the characteristic SFR of a halo increases smoothly with increasing halo mass (Fig. 7). BHs in haloes of mass $M_{200} \lesssim 10^{11.5}$ M$_{\odot}$ accrete at a 'low' rate ($\dot{M}_{\mathrm{BH}} < 10^{-4}$ M$_{\odot}$ yr^{-1}). They then transition through haloes of mass $10^{11.5} \sim 10^{12.5}$ M$_{\odot}$ to a 'high' rate ($\dot{M}_{\mathrm{BH}} > 10^{-4}$ M$_{\odot}$ yr^{-1}) in haloes of mass $M_{200} \gtrsim 10^{12.5}$ M$_{\odot}$. However, the scatter in the BHAR at fixed halo mass is very large (up to $\sim$6 dex). Galaxies with SFRs far below the characteristic SFR all contain massive BHs ($M_{\mathrm{BH}} \geq 10^7$ M$_{\odot}$).

(v) The median evolutionary trend for a galaxy's SFR and the accretion rate of its central BH, averaged over 100 Myr, are insensitive to the final properties of the system (Fig. 9). By equating these trends together we found that the 100 Myr average SFR as a function of the 100 Myr average BHAR can be split into three regimes, separated by the halo mass (Fig. 10). BHs hosted by haloes below the characteristic transition mass, M_{crit} (B17, $M_{200} \sim 10^{12}$ M$_{\odot}$), fail to grow effectively, yet the galaxy continues to grow with the halo. Once the halo reaches M_{crit} there is a non-linear 'switch' of BH growth that rapidly builds the mass of the BH. In the most massive haloes ($M_{200} > M_{\mathrm{crit}}$) both SFR and BHAR decline on average, with a roughly constant scaling of SFR/BHAR $\sim 10^3$.

REFERENCES

Aird J. et al., 2010, MNRAS, 401, 2531
Alexander D. M., Hickox R. C., 2012, New Astron. Rev., 56, 93
Azadi M. et al., 2015, ApJ, 806, 187
Bahé Y. M. et al., 2016, MNRAS, 456, 1115
Barber C., Schaye J., Bower R. G., Crain R. A., Schaller M., Theuns T., 2016, MNRAS, 460, 1147
Bondi H., Hoyle F., 1944, MNRAS, 104, 273
Booth C. M., Schaye J., 2009, MNRAS, 398, 53
Booth C. M., Schaye J., 2010, MNRAS, 405, L1
Booth C. M., Schaye J., 2011, MNRAS, 413, 1158
Bower R. G., Schaye J., Frenk C. S., Theuns T., Schaller M., Crain R. A., McAlpine S., 2017, MNRAS, 465, 32 (B17)
Chang Y.-Y., van der Wel A., da Cunha E., Rix H.-W., 2015, ApJS, 219, 8
Chen C.-T. J. et al., 2013, ApJ, 773, 3
Correa C. A., Wyithe J. S. B., Schaye J., Duffy A. R., 2015, MNRAS, 450, 1521
Crain R. A. et al., 2015, MNRAS, 450, 1937
Crain R. A. et al., 2017, MNRAS, 464, 4204
Dalla Vecchia C., Schaye J., 2012, MNRAS, 426, 140
Davis M., Efstathiou G., Frenk C. S., White S. D. M., 1985, ApJ, 292, 371
Delvecchio I. et al., 2015, MNRAS, 449, 373
Di Matteo T., Springel V., Hernquist L., 2005, Nature, 433, 604
Dolag K., Borgani S., Murante G., Springel V., 2009, MNRAS, 399, 497
Dubois Y., Volonteri M., Silk J., Devriendt J., Slyz A., Teyssier R., 2015, MNRAS, 452, 1502
Elbaz D. et al., 2007, A&A, 468, 33
Furlong M. et al., 2015, MNRAS, 450, 4486
Furlong M. et al., 2017, MNRAS, 465, 722
Greene J. E. et al., 2016, ApJ, 826, L32
Gutcke T. A., Fanidakis N., Macciò A. V., Lacey C., 2015, MNRAS, 451, 3759
Haardt F., Madau P., 2001, in Neumann D. M., Tran J. T. V., eds, Clusters of Galaxies and the High Redshift Universe Observed in X-rays. http://moriond.in2p3.fr
Habouzit M., Volonteri M., Dubois Y., 2017, MNRAS, in press
Harrison C. M. et al., 2012, ApJ, 760, L15
Heckman T. M., Kauffmann G., Brinchmann J., Charlot S., Tremonti C., White S. D. M., 2004, ApJ, 613, 109
Hickox R. C., Mullaney J. R., Alexander D. M., Chen C.-T. J., Civano F. M., Goulding A. D., Hainline K. N., 2014, ApJ, 782, 9
Hopkins P. F., Hernquist L., Cox T. J., Di Matteo T., Martini P., Robertson B., Springel V., 2005, ApJ, 630, 705
Hopkins P. F., Hernquist L., Cox T. J., Kereš D., 2008, ApJS, 175, 356
Jahnke K., Macciò A. V., 2011, ApJ, 734, 92
Kormendy J., Ho L. C., 2013, ARA&A, 51, 511
Lagos C. d. P. et al., 2015, MNRAS, 452, 3815
Lutz D. et al., 2010, ApJ, 712, 1287
McAlpine S. et al., 2016, Astron. Comput., 15, 72
McConnell N. J., Ma C.-P., 2013, ApJ, 764, 184
Madau P., Dickinson M., 2014, ARA&A, 52, 415
Magorrian J. et al., 1998, AJ, 115, 2285
Mullaney J. R. et al., 2012a, MNRAS, 419, 95
Mullaney J. R. et al., 2012b, ApJ, 753, L30
Neistein E., Netzer H., 2014, MNRAS, 437, 3373
Page M. J. et al., 2012, Nature, 485, 213
Peng C. Y., 2007, ApJ, 671, 1098
Planck Collaboration I, 2014, A&A, 571, A1

Pontzen A., Tremmel M., Roth N., Peiris H. V., Saintonge A., Volonteri M., Quinn T., Governato F., 2017, MNRAS, 465, 547
Qu Y. et al., 2017, MNRAS, 464, 1659
Rafferty D. A., Brandt W. N., Alexander D. M., Xue Y. Q., Bauer F. E., Lehmer B. D., Luo B., Papovich C., 2011, ApJ, 742, 3
Rahmati A., Schaye J., Bower R. G., Crain R. A., Furlong M., Schaller M., Theuns T., 2015, MNRAS, 452, 2034
Reines A. E., Volonteri M., 2015, ApJ, 813, 82
Rosario D. J. et al., 2012, A&A, 545, A45
Rosas-Guevara Y. M. et al., 2015, MNRAS, 454, 1038
Rosas-Guevara Y., Bower R. G., Schaye J., McAlpine S., Dalla Vecchia C., Frenk C. S., Schaller M., Theuns T., 2016, MNRAS, 462, 190
Sanders D. B., Soifer B. T., Elias J. H., Madore B. F., Matthews K., Neugebauer G., Scoville N. Z., 1988, ApJ, 325, 74
Schaller M. et al., 2015a, MNRAS, 451, 1247
Schaller M., Dalla Vecchia C., Schaye J., Bower R. G., Theuns T., Crain R. A., Furlong M., McCarthy I. G., 2015b, MNRAS, 454, 2277
Schaye J., Dalla Vecchia C., 2008, MNRAS, 383, 1210
Schaye J. et al., 2015, MNRAS, 446, 521
Scott N., Graham A. W., Schombert J., 2013, ApJ, 768, 76
Segers M. C., Crain R. A., Schaye J., Bower R. G., Furlong M., Schaller M., Theuns T., 2016, MNRAS, 456, 1235
Shakura N. I., Sunyaev R. A., 1973, A&A, 24, 337
Sijacki D., Vogelsberger M., Genel S., Springel V., Torrey P., Snyder G. F., Nelson D., Hernquist L., 2015, MNRAS, 452, 575
Springel V., 2005, MNRAS, 364, 1105
Springel V., White S. D. M., Tormen G., Kauffmann G., 2001, MNRAS, 328, 726
Springel V., Di Matteo T., Hernquist L., 2005, MNRAS, 361, 776
Stanley F., Harrison C. M., Alexander D. M., Swinbank A. M., Aird J. A., Del Moro A., Hickox R. C., Mullaney J. R., 2015, MNRAS, 453, 591
Symeonidis M. et al., 2011, MNRAS, 417, 2239
Thacker R. J., MacMackin C., Wurster J., Hobbs A., 2014, MNRAS, 443, 1125
Trayford J. W. et al., 2015, MNRAS, 452, 2879
Trayford J. W., Theuns T., Bower R. G., Crain R. A., Lagos C. d. P., Schaller M., Schaye J., 2016, MNRAS, 460, 3925
Volonteri M., Capelo P. R., Netzer H., Bellovary J., Dotti M., Governato F., 2015a, MNRAS, 449, 1470
Volonteri M., Capelo P. R., Netzer H., Bellovary J., Dotti M., Governato F., 2015b, MNRAS, 452, L6
Wiersma R. P. C., Schaye J., Smith B. D., 2009a, MNRAS, 393, 99
Wiersma R. P. C., Schaye J., Theuns T., Dalla Vecchia C., Tornatore L., 2009b, MNRAS, 399, 574

APPENDIX A: PREDICTIONS FROM THE INTEGRATED QUANTITIES

The major motivation for linking the growth of galaxies to the growth of their central BH has arisen empirically from the strong correlations seen in their integrated properties (the primary example being the tight $M_{\rm BH}$–$M_{\rm *,\,bulge}$ relation). We therefore require an evolutionary model that suitably fits this end point. In the simplest case, where BHs and their host galaxy grow in concert (or co-evolve), the relational form between their growth rates can be easily predicted. Given a functional form of the $M_{\rm BH}$–$M_{\rm bulge,\,*}$ relation described via

$$\log_{10} M_{\rm BH} = \alpha \log_{10} M_{\rm bulge,*} + \log_{10}\beta, \qquad (A1)$$

where α is the gradient of the slope and $\log_{10}\beta$ is the intercept, the predicted relation between the growth rates is simply found by differentiating with respect to time, i.e.

$$\log_{10}\dot{M}_{\rm BH} = \log_{10}\dot{M}_{\rm bulge,*} + \log_{10}\beta + \log_{10}\alpha + (\alpha-1)\log_{10} M_{\rm bulge,*}. \qquad (A2)$$

In the trivial case where $\alpha = 1$ (i.e. a linear relation) this reduces to

$$\log_{10}\dot{M}_{\rm BH} = \log_{10}\dot{M}_* + \log_{10}\beta. \tag{A3}$$

Within this scenario, growth rates are directly proportional to one another scaled by the intercept, β, of the $M_{\rm BH}$–$M_{\rm bulge,\,*}$ relation. Therefore, if the functional form between the growth rates is described via

$$\log_{10}\dot{M}_{\rm BH} = \gamma\log_{10}\dot{M}_* + \log_{10}\delta, \tag{A4}$$

where again γ and δ are the slope and intercept values, we would expect $\delta = \beta$ and $\gamma = 1$ in the case where $\alpha = 1$.

Throughout this study, we will test the hypothesis that there exists a broadly linear co-evolution between galaxies and their central BHs, a plausible scenario fitting the empirical $M_{\rm BH}$–$M_{*,\,\rm bulge}$ relation. We refer throughout to α as the gradient of the slope between the integrated properties ($M_{\rm BH}$–$M_{*/\rm bulge,\,*}$) and to γ as the slope between each growth rate ($\dot{M}_{\rm BH}$–$\dot{M}_*$), both in log space.

This paper has been typeset from a TeX/LaTeX file prepared by the author.